Research Article

Journal of Environmental Nanotechnology

Synthesis of *Bougainvillea spectabilis* Leaf Extract-mediated ZnO, MgO and CuO Nanoparticles

M. R. Chitra Devi* and B. Ramesh
Department of Biochemistry, PSG College of Arts and Science, Coimbatore, TN, India
Received: 02.01.2026 Accepted: 05.02.2026 Published: 30.03.2026
*chitraratheesh@gmail.com

ABSTRACT

In this research work, *Bougainvillea spectabilis* leaf extract-mediated ZnO, MgO and CuO nanoparticles were synthesized by green synthesis. Due to the presence of phytochemical compounds like saponins, alkaloids etc., *Bougainvillea spectabilis* leaf extract was utilized as a stabilizing and reducing agent. X-ray diffraction, UV-Visible spectroscopy, scanning electron microscopy and Fourier Transform infrared spectroscopy were the characterization techniques used for analyzing the samples. Crystalline size of the prepared samples was determined by X-ray diffraction method and functional groups were confirmed by FT-IR spectroscopy. The presence of elements in the prepared samples was revealed by SEM-EDAX studies. The optical properties of the nanoparticles were studied by UV-Visible spectroscopy in the range 200-800 nm. The antidiabetic activity of the metal oxide nanoparticles was also studied.

Keywords: *Bougainvillea spectabilis*; Metal oxide nanoparticles; Antidiabetic activity; Plant-assisted synthesis.

1. INTRODUCTION

Nanotechnology is growing fast and has gained interest in the past two decades. It has numerous uses in research, development, and industry (Alabur *et al.* 2016). Green synthesis of metal oxide nanoparticles *via* plant extracts has emerged as a cost-effective and eco-friendly approach. This technique exploits the rich phytochemical content of plants, which can be used as natural capping, stabilizing, and reducing agents. *Bougainvillea spectabilis*, a widely distributed ornamental plant, is recognized for its vibrant flowers and medicinal properties. Its flower extract contains a variety of bioactive compounds, including flavonoids, tannins, alkaloids, and phenolics, which are effective in mediating the combination of metal oxide nanoparticles under mild circumstances without the use of toxic chemicals (Chauhan *et al.* 2024, Ali *et al.* 2023).

ZnO nanoparticles typically exhibit a hexagonal wurtzite structure with a strong UV absorption peak around 308 nm, attributed to band-to-band electronic transitions and the quantum confinement effect (Ramesh *et al.* 2015). CuO nanoparticles synthesized through this green method display a monoclinic phase and an absorption peak at approximately 310 nm, indicative of Cu^{2+} to O^{2-} charge transfer and d–d transitions (Rotti *et al.* 2023). MgO nanoparticles, on the other hand, show a cubic crystal structure with an absorption peak near 307 nm and characteristic Mg–O vibrational bands, as established by FTIR investigation (Patil *et al.* 2016). In the present work, ZnO, CuO, and MgO nanoparticles were synthesized *via Bougainvillea spectabilis* leaf extract. These findings attest the effectiveness of *Bougainvillea spectabilis* flower extract as a natural and sustainable mediator for the biosynthesis of high-quality metal oxide nanoparticles.

2. MATERIALS AND METHODS

2.1 Materials

Fresh *Bougainvillea spectabilis* leaves were collected locally, carefully cleaned with distilled water to eliminate dust and impurities, and air-dried under shade at room temperature. Analytical grade precursors including zinc acetate dihydrate ($Zn(CH_3COO)_2{\cdot}2H_2O$), copper(II) acetate monohydrate ($Cu(CH_3COO)_2{\cdot}H_2O$), and magnesium acetate tetrahydrate ($Mg(CH_3COO)_2{\cdot}4H_2O$) were obtained from Sigma-Aldrich and used without further purification. All solutions were prepared using double-distilled water.

2.2 Preparation of *Bougainvillea* Flower Extract

About 10 g of dried *Bougainvillea spectabilis* leaves were boiled in 100 mL of distilled water at 80°C for 30 minutes. The extract was filtered using Whatman No. 1 filter paper and kept at 4°C for further use. This extract served as the natural reducing and stabilizing agent in the sol-gel synthesis.

2.3 Synthesis of ZnO Nanoparticles

$Zn(COOCH_3)_2{\cdot}2H_2O$ (0.1 M) was dissolved in 50 mL of distilled water and stirred magnetically at room temperature. About 20 mL of bougainvillea leaf extract was added dropwise under continuous stirring. The pH

was adjusted to 12 using 1 M NaOH to promote gel formation. The resulting sol was stirred at 70°C until it transformed into a viscous gel. The gel was dehydrated in an oven at 100°C to obtain a solid precursor. The dried material was calcined at 400°C for 2 hours to obtain ZnO nanoparticles.

2.4 Synthesis of CuO Nanoparticles

$Cu(COOCH_3)_2{\cdot}H_2O$ (0.1 M) was dissolved in 50 mL distilled water. About 20 mL of the leaf extract was added slowly under constant stirring. The pH was raised to 12 using NaOH, initiating the sol-gel transition. The sol was aged and heated at 70°C to form a stable gel. The gel was dried and then calcined at 450°C for 2 hours to yield CuO nanoparticles.

2.5 Synthesis of MgO Nanoparticles

$Mg(COOCH_3)_2{\cdot}4H_2O$ (0.1 M) was dissolved in 50 mL of water with vigorous stirring. About 20 mL of the leaf extract was added dropwise. The pH was adjusted to 12, and the sol was heated to form a gel. After gelation, the sample was dried and calcined at 500°C for 2 hours to obtain MgO nanoparticles.

2.6 Characterization Techniques

The synthesized nanoparticles were characterized by X-ray Diffraction (XRD) for phase identification and crystallite size estimation, UV-Visible Spectroscopy (UV-Vis) for optical property analysis, Fourier Transform Infrared Spectroscopy (FTIR) to spot functional groups from the plant extract, Scanning Electron Microscopy (SEM) for morphology examination, Energy Dispersive X-ray Spectroscopy (EDAX) for elemental composition analysis, Antidiabetic assays for α-amylase and α-glucosidase inhibition studies.

2.7 Antidiabetic Assays

2.7.1 Determination of α-Amylase Inhibitory Activity

The extract of *Bougainvillea spectabilis* was dissolved in buffer (NaCl 0.006 M, Na_2HPO_4/NaH_2PO_4 0.02 M) at pH 6.9 to make the concentrations (15.625 to 500 µg/mL). About 200 µL of α-amylase solution (2 units/mL) was mixed with 200 µL of the crude extract and solvent fractions and incubated for about 10 minutes at 30°C. Subsequently, 200 µL of 1% starch solution was added to each tube and incubated for about 3 minutes. Then, the reaction was terminated by adding 200 µL of DNSA reagent, followed by boiling in a water bath at 85 °C for approximately 10 minutes. Finally, the mixture was cooled to ambient temperature and diluted with 5 mL of distilled water, and the absorbance was determined at 540 nm using a UV-visible spectrophotometer. The blank with 100% enzyme activity was prepared by substituting the extract with 200 µL of the buffer. A blank with the plant extract at each concentration was used in the absence of the enzyme solution.

$$\%\ inhibition = \frac{Abs\ of\ control - Abs\ of\ sample\ treated\ with\ extract}{Abs\ of\ control} \times 100$$

2.7.2 Determination of α-Glucosidase Inhibition Assay

The α-glucosidase inhibitory effect of the crude extract of *Bougainvillea spectabilis* and solvent fractions was evaluated by using *p*-nitro-phenyl-a-D glucopyranoside (*p*-NPG) substrate solution (using 0.1 M potassium phosphate buffer, pH 6.8). Similarly, 0.1 unit/mL of α-glucosidase was dissolved using potassium phosphate buffer. All the samples were dissolved in dimethyl sulfoxide, and 20 mL of each sample was mixed with the same volume of enzyme solution. Subsequently, a volume of 40 mL substrate solution was added for initiation of the reaction and incubated at 37°C for 40 minutes. Then, 80 mL of 0.2 M sodium carbonate in phosphate buffer, pH 6.8 was added to terminate the reaction. Finally, the amount of released *p*-nitrophenol (*p*-NP) was measured at 405 nm.

$$\%\ inhibition = \frac{Abs\ of\ control - Abs\ of\ sample\ treated\ with\ extract}{Abs\ of\ control} \times 100$$

3. RESULT AND DISCUSSION

3.1 X-ray Diffraction Analysis

The XRD pattern of the biosynthesized ZnO nanoparticles is shown in the Fig. 1. According to JCPDS card No: 50-0664, the crystalline peaks seen at 31.67°, 34.31°, 36.14°, 47.40°, 56.52°, 62.73° and 66.28° correspond to (100), (002), (101), (102), (110), (103) and (112) hkl planes, respectively. No characteristic peaks of any impurities were noticed suggesting the high quality of ZnO nanoparticles (Xuan *et al.* 2024). The crystallite size (D) of the nanoparticles was calculated using Debye Scherrer's formula ($D = k\lambda/\beta\cos\theta$), where λ represents the wavelength of X-rays (1.5406 Å), β denotes the full width at half maximum (FWHM) of diffraction peaks and θ = is the diffracted angle of X-rays. The average crystallite size of ZnO nanoparticles is 37.78 nm.

The XRD pattern of biosynthesized CuO nanoparticles exhibits characteristic sharp peaks at specific 2θ angles corresponding to their monoclinic crystal structure, consistent with JCPDS card No. 48-1548 (ICDD 1977). The identified peaks, labeled with Miller indices (110), (002), and (111), confirm the phase purity and high crystallinity of the sample, indicating well-ordered atomic planes within the lattice (Cullity and Stock, 2001). These diffraction peaks result from constructive interference of X-rays reflected by the crystal planes, and their positions align with reported CuO lattice parameters (Vella *et al.* 2019).

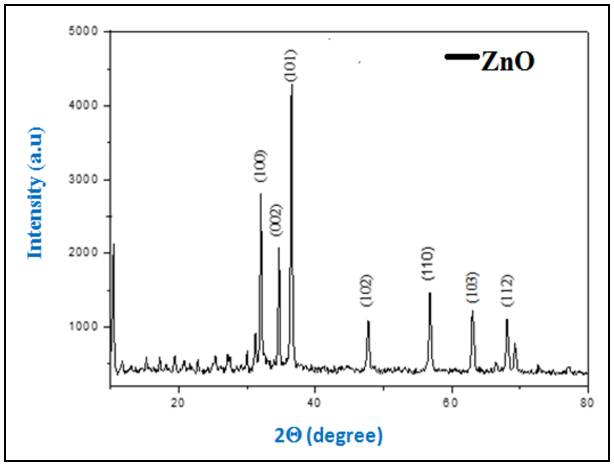


Fig. 1: XRD graph of biosynthesized ZnO nanoparticles

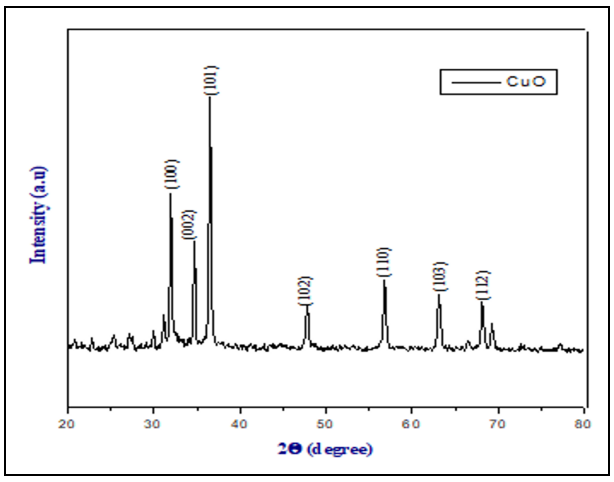


Fig. 2: XRD graph of biosynthesized CuO nanoparticles

The X-ray diffraction pattern of MgO nanoparticles shown in Fig. 3 exhibits distinct peaks at various 2θ values corresponding to the characteristic crystallographic planes of the MgO cubic crystal structure. The peaks corresponding to (100), (002), (101), (110), (103), and (112) indicate a well-defined crystalline phase with high purity and crystallinity. These diffraction peaks match the standard MgO pattern (typically matching JCPDS card no. 45-0946), confirming the formation of magnesium oxide with a rock-salt cubic structure. The sharpness and intensity of the peaks suggest good crystallite size and minimal lattice strain, which are indicative of high-quality MgO nanoparticles. (Marwaha *et al.* 2017).

3.2 UV-vis Spectroscopy Analysis

The UV-Vis absorption spectrum of the biosynthesized ZnO nanoparticles exhibits a strong absorption band at 308 nm (Fig. 4). This absorption is due to the intrinsic band-to-band transition in ZnO nanoparticles and is indicative of successful nanoparticle formation. This band shows a blue shift compared to bulk ZnO, which typically absorbs at ~365 nm. This shift is ascribed to the quantum confinement effect arising from the nanoscale size of the particles. The intensity of the absorption band also indicates good crystallinity and high purity of the synthesized nanoparticles (Ahamed *et al.* 2023).

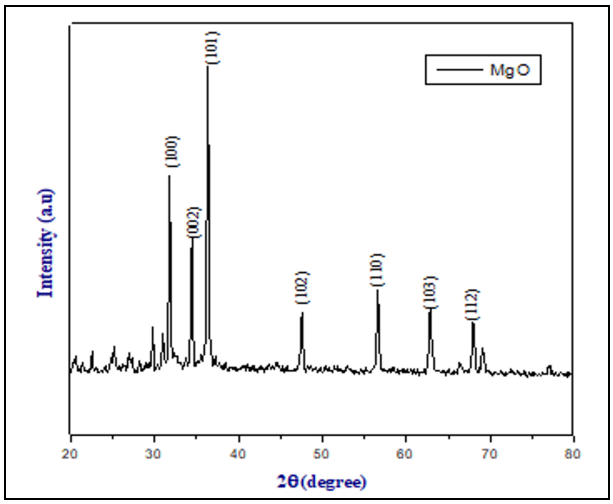


Fig. 3: XRD pattern of biosynthesized MgO nanoparticles

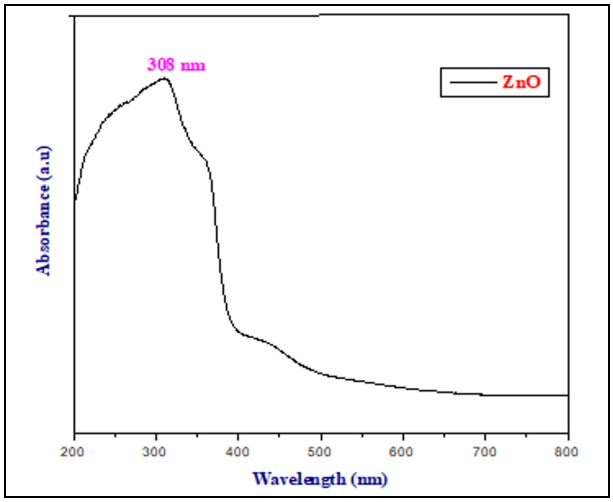


Fig. 4: UV spectrum of biosynthesized ZnO nanoparticles

The UV-Vis spectrum of biosynthesized CuO nanoparticles shows a notable absorption band at 310 nm, confirming successful synthesis and characteristic optical behavior of CuO in nanoscale form (Fig. 5). The absorption at 310 nm indicates electronic transitions related to the $Cu^{2+} \rightarrow O^{2-}$ charge transmission and possible d–d transitions, typical of monoclinic CuO nanostructures (Zaman *et al.* 2012).

The UV-Vis absorption spectrum of biosynthesized MgO nanoparticles shows a discrete absorption band at 307 nm, which is consistent with the typical optical properties of nanoscale magnesium oxide (Fig. 6). This band indicates strong electronic transitions

in the ultraviolet region. It lies within the expected range for MgO, which generally absorbs in the 200–320 nm region. The steep decline after 307 nm and flat absorption through the visible range confirm that the particles primarily absorb UV radiation, and remain transparent in the visible region, characteristic insulating behavior of MgO (Nguyen *et al.* 2020).

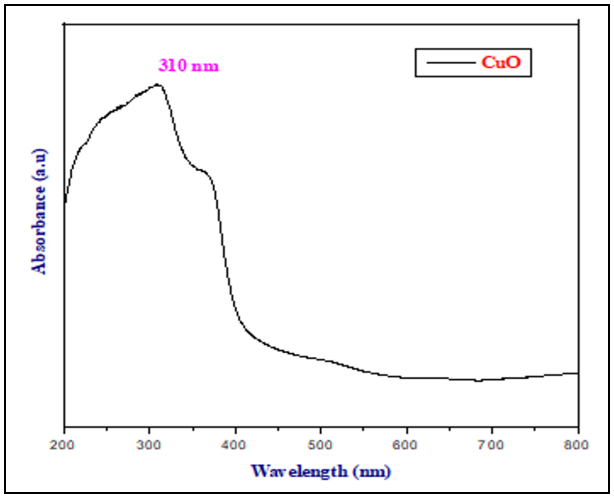


Fig. 5: UV spectrum of biosynthesized CuO nanoparticles

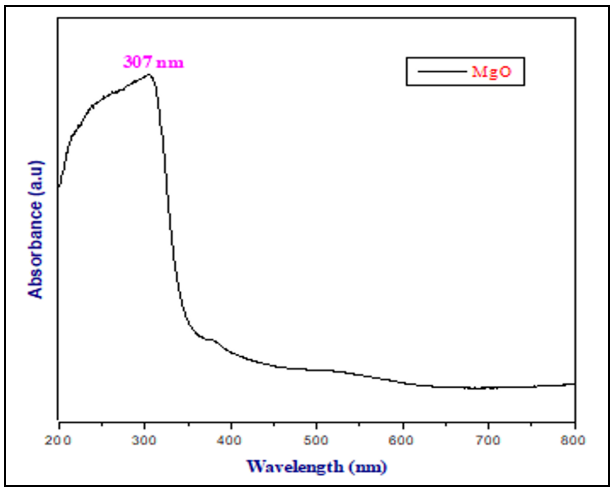


Fig. 6: UV spectrum of biosynthesized MgO nanoparticles

3.3 Scanning Electron Microscope Analysis

The shape and regular grain size of the prepared samples were found using SEM analysis. The SEM images of ZnO, CuO and MgO nanoparticles are shown in Fig. 7 (a-c). The ZnO sample reveals hexagonal and irregular-shaped particles with a relatively uniform distribution, consistent with its typical wurtzite structure. The SEM image of CuO nanoparticles shows a denser agglomeration of fine, nearly spherical nanoparticles, suggesting a high surface area and porosity. The MgO sample exhibits a relatively coarse texture with clustered granular particles, indicating crystallite formation and possible sintering during synthesis. These morphological characteristics are in agreement with prior studies on ZnO, CuO and MgO (Raliya *et al.* 2016; Sankar *et al.* 2014).

3.4 FTIR Analysis

The functional groups in the ZnO, CuO and MgO particles prepared from the leaf extract of *Bougainvillea spectabilis* were noted using FTIR analysis. The spectra were recorded from 4000 cm^{-1} to 400 cm^{-1}.

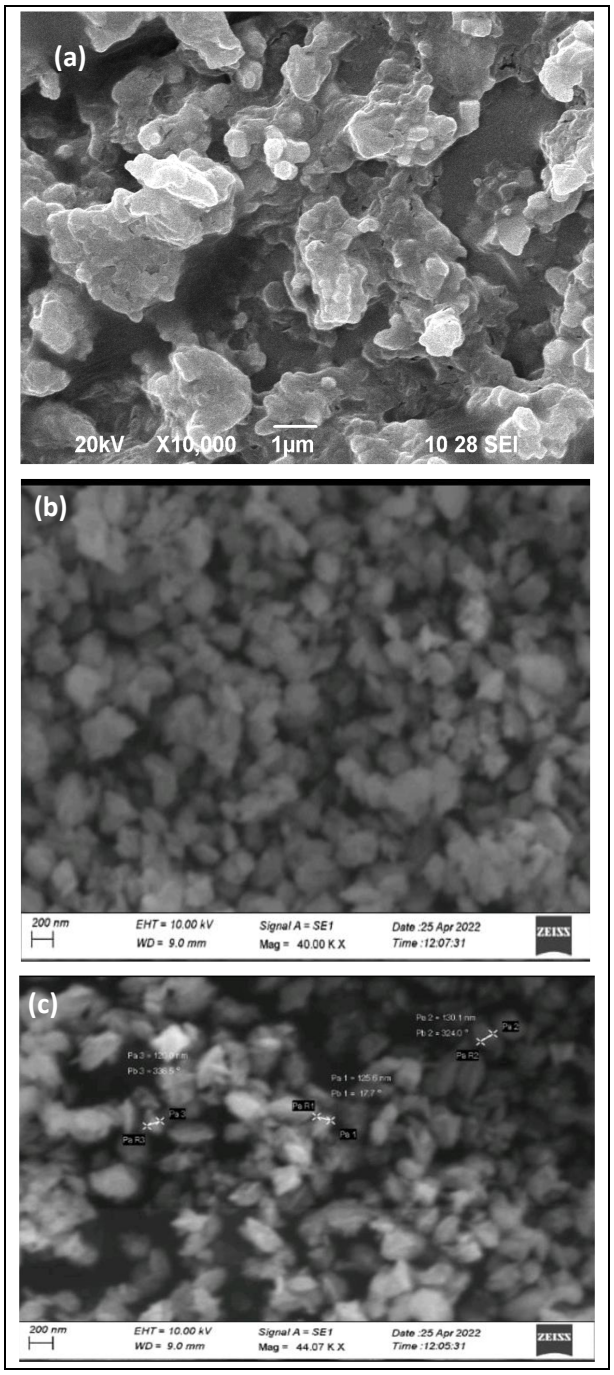


Fig. 7: SEM images of biosynthesized (a) ZnO nanoparticles (b) CuO nanoparticles and (c) MgO nanoparticles

In the IR spectrum of ZnO nanoparticles (Fig. 8), the peak at 3861 cm^{-1} represents stretching vibration of O-H from phenolic compounds present in the plant (Najamul *et al.* 2023; Abdelkhalek *et al.* 2020). The peak at 2315 cm^{-1} was assigned to C=N stretching of nitriles (Munisha *et al.* 2025). The peak at 1687 cm^{-1} is due to C═C stretching of the alkene group (Amani *et al.* 2022). The peak at 1553 cm^{-1} corresponds to the N-H bond of primary amines and stretching C–C (Fouda *et al.* 2023). The peak at 1418 cm^{-1} reveals the C=O stretching vibrations (Sankar *et al.* 2014). The Zn-O bond is observed at 646 cm^{-1} (Prashantkumar *et al.* 2025).

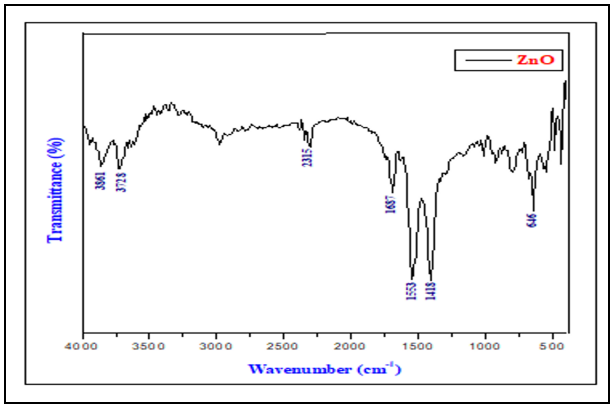


Fig. 8: FTIR spectrum of biosynthesized ZnO nanoparticles

The FTIR spectrum of CuO nanoparticles (Fig. 9) shows characteristic absorption peaks that confirm the presence of copper oxide. In the spectrum, peaks observed at 591 cm^{-1} and 867 cm^{-1} correspond to Cu–O stretching vibrations, which are indicative of CuO formation. The broad peak at 3831 cm^{-1} is accredited to O–H stretching vibrations from adsorbed moisture or surface hydroxyl groups. The peak at 1439 cm^{-1} may be due to carbonate impurities or surface-adsorbed species. These observations align with reported studies on CuO nanoparticles, which identify metal-oxygen vibrational modes in the 500–700 cm^{-1} range and hydroxyl groups at higher wavenumbers (Dhineshbabu *et al.* 2016).

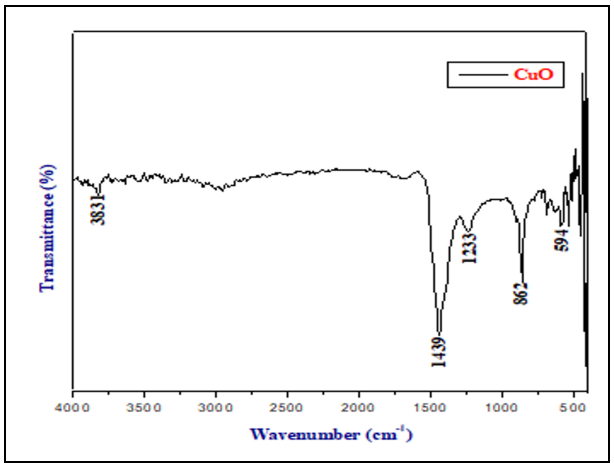


Fig. 9: FTIR spectrum of biosynthesized CuO nanoparticles

The FTIR spectrum of biosynthesized MgO nanoparticles (Fig. 10) displays several characteristic absorption bands confirming the presence of functional groups present in the synthesis and stabilization process. A broad peak around 3406 cm^{-1} is due to O–H stretching vibrations, indicating the presence of hydroxyl groups, which may originate from plant extracts or water molecules adsorbed on the nanoparticle surface. The peak observed at 1635 cm^{-1} is ascribed to the bending vibration of H–O–H, further supporting the presence of moisture. The peak at 1449 cm^{-1} could be due to C–H bending vibrations indicating the presence of organic biomolecules acting as capping agents. A prominent band at 439 cm^{-1} is representative of the Mg–O stretching vibration, confirming the formation of magnesium oxide nanoparticles. These findings are in line with earlier reports on the FTIR characterization of green-synthesized MgO nanoparticles (Chauhan *et al.* 2024, Ali *et al.* 2023).

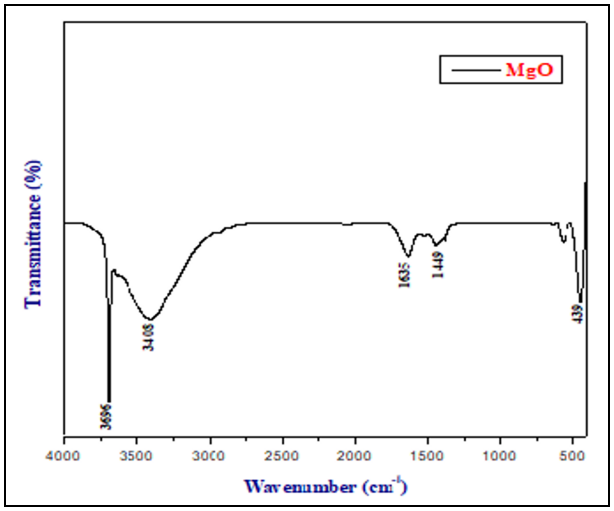


Fig. 10: FTIR spectrum of biosynthesized MgO nanoparticles

3.5 Energy Dispersive X-ray Spectroscopy (EDAX)

The EDAX spectra of biosynthesized ZnO and CuO nanoparticles in Fig. 11-13 confirm the elemental compositions of the samples. For ZnO, strong signals corresponding to Zn and O validate the successful formation of ZnO nanoparticles with minimal impurities. In the CuO spectrum (Fig. 12), dominant peaks for Cu and O affirm the formation of CuO, with a minor presence of Na, likely introduced *via* the plant extract used during synthesis. For CuO (Fig. 13), peaks for O, C, Mg, Cl, and K were observed. The O and Cu peaks confirm the presence of CuO, while C, Si, Y, Mg, Cl, and K are possibly residual phytochemicals or biomolecules from the green synthesis process, often acting as reducing and stabilizing agents. These results emphasize the role of phytochemicals in nanoparticle stabilization and align with literature reporting the successful use of plant-

mediated synthesis for metal oxide nanoparticles (Sankar *et al.* 2014; Panchal *et al.* 2022).

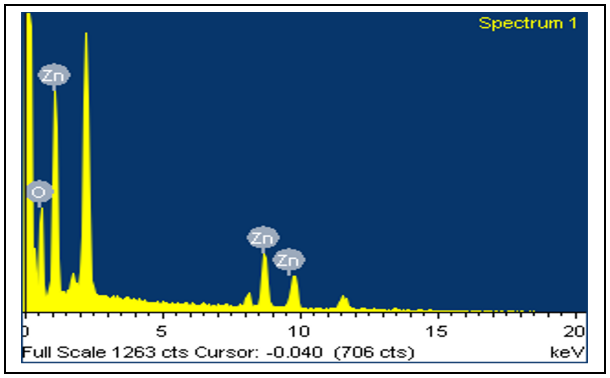


Fig. 11: EDAX spectrum of biosynthesized ZnO nanoparticles

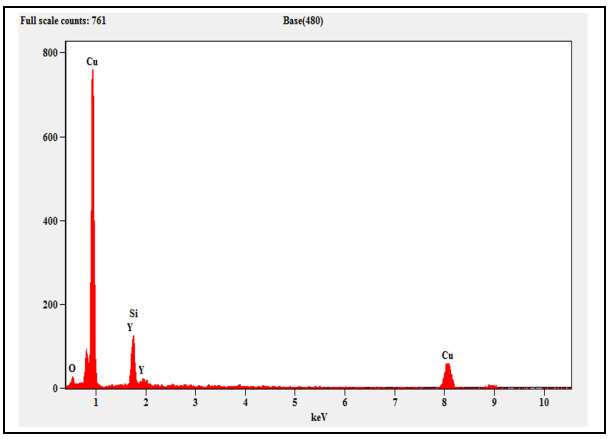


Fig. 12: EDAX spectrum of biosynthesized CuO nanoparticles

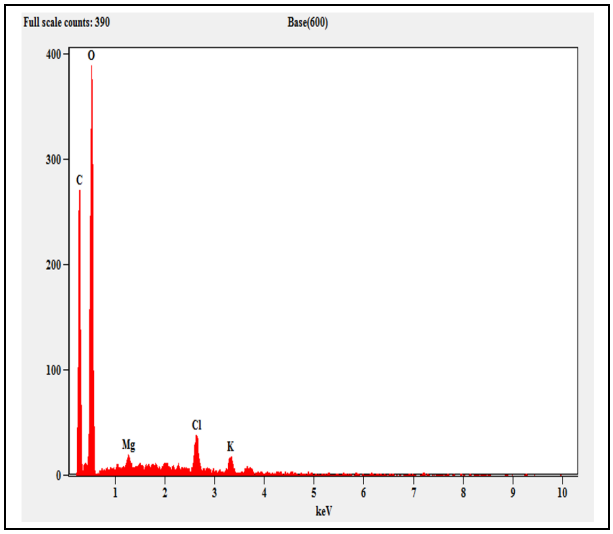


Fig. 13: EDAX spectrum of biosynthesized CuO nanoparticles

3.6 Antidiabetic Activity

The antidiabetic potential of the biosynthesized nanoparticles was evaluated by their inhibitory effects on two key carbohydrate-hydrolyzing enzymes: α-amylase and α-glucosidase. As shown in Table 1, all nanoparticles exhibited dose-dependent inhibition of α-amylase, with CuO nanoparticles achieving the highest inhibition (76.60%) at 100 µL, followed by MgO (58.67%) and ZnO (52.08%). These values, although lower than that of the standard acarbose (82.61%), demonstrate significant enzyme-inhibitory activity, particularly for CuO, which closely approaches the standard drug.

Table 1. α-Amylase inhibition studies

S. No.	Sample Concentration (µL)	Acarbose Standard	% of α-amylase Inhibitory Activity (CuO)	% of α-amylase Inhibitory Activity (MgO)	% of α-amylase Inhibitory Activity (ZnO)
1	20	25.00 %	17.45 %	19.20%	15.23%
2	40	34.02 %	33.35 %	26.54%	28.63%
3	60	65.73 %	42.00 %	38.06%	32.41%
4	80	73.83 %	53.97 %	42.64%	45.21%
5	100	82.61 %	76.60 %	58.67%	52.08%

Similarly, the α-glucosidase inhibition assay (Table 2) revealed notable enzyme inhibition by all three nanoparticles. At 100 µL, CuO again showed the highest inhibition (78.06%), followed by MgO (70.69%) and ZnO (63.25%), compared to that of acarbose (98.52%). The consistent performance of CuO across both assays suggests superior bioactivity, potentially due to their surface reactivity and phytochemical capping agents from *Bougainvillea spectabilis* extract. These findings reinforce the therapeutic activity of green-synthesized metal oxide nanoparticles as alternative antidiabetic agents by delaying carbohydrate digestion and glucose absorption through effective enzyme inhibition (Raliya *et al.* 2016).

Table 2. α -Glucosidase inhibition studies

S. No.	Sample Concentration (µL)	Acarbose Standard	% of α-glucosidase Inhibitory Activity (CuO)	% of α-glucosidase Inhibitory Activity (MgO)	% of α-glucosidase Inhibitory Activity (ZnO)
1	20	40.73 %	22.36 %	27.34 %	19.32%
2	40	49.34 %	42.60 %	35.63 %	28.54%
3	60	63.48 %	55.20 %	48.95 %	37.41%
4	80	72.56 %	67.58 %	65.01 %	51.14%
5	100	98.52 %	78.06 %	70.69 %	63.25%

4. CONCLUSION

In this study, ZnO, CuO and MgO nanoparticles were successfully synthesized using *Bougainvillea spectabilis* leaf extract *via* a green synthesis method. Structural and morphological analyses using XRD, SEM, and FTIR revealed the formation of crystalline, phase-pure nanoparticles, with ZnO showing a hexagonal wurtzite structure, CuO exhibiting a monoclinic phase, and MgO displaying a cubic crystal structure. UV–visible spectroscopy indicated absorption bands in the UV region, consistent with nanoscale optical behaviour and good crystallinity. The FTIR spectrum revealed functional groups from phytochemicals, supporting their role in capping and stabilizing the nanoparticles.

The biosynthesized nanoparticles exhibited promising antidiabetic activity through *in vitro* α-amylase and α-glucosidase inhibition assays. Among the samples, CuO nanoparticles demonstrated the highest inhibitory potential in both assays, nearing the performance of the standard drug Acarbose. These findings highlight the effectiveness of *Bougainvillea spectabilis* leaf extract not only as a green synthesis agent but also as a contributor to the therapeutic potential of the nanoparticles. Overall, this work reinforces the value of plant-mediated nanomaterials as eco-friendly and biologically active agents for future biomedical and pharmaceutical applications.

ACKNOWLEDGEMENTS

The authors are thankful to the ABR College of Engineering and Technology for infrastructure, lab facilities, and constant support for this research work.

FUNDING

This research received no specific grant from any funding agency in the public, commercial, or not-for-profit sectors.

CONFLICTS OF INTEREST

The authors declare that there is no conflict of interest to publish this paper.

COPYRIGHT

This article is an open-access article distributed under the terms and conditions of the Creative Commons Attribution (CC BY) license (http://creativecommons.org/licenses/by/4.0/).

REFERENCE

Abdelkhalek, A. and Alaskar, A. A., Green Synthesized ZnO Nanoparticles Mediated by Mentha Spicata Extract Induce Plant Systemic Resistance against Tobacco Mosaic Virus, *Appl. Sci.,* 10(15), 5054(2020). https://doi.org/10.3390/app10155054

Ahamed, M., Akhtar, M. J. and Khan, M. A. M., Green-fabricated MgO nanoparticles: a potent antimicrobial and anticancer agent, *J. King Saud Univers. Sci.,* 35, 102889(2023). https://doi.org/10.1016/j.jksus.2023.102889

Alabur, M., Irfan, M., Anushree, K. P., Vinutha, K. M. and Yamunarani, N., Synthesis and characterization of CuO Nanoparticles and CuO doped PVA Nanocomposites, *Adv. Mater. Phys. Chem.,* 6(10), 263-273(2016). https://doi.org/10.4236/ampc.2016.610026

Ali, M. M., Al-Qahtani, A., Alharthi, S. S., Anwar, A., Alhoshani, A., Barakat, A. and Alshahrani, M. M., Exploring the antibacterial potential of green-synthesized MgO and ZnO nanoparticles from two plant root extracts, *Nanomater.,* 13(11),1740(2023). https://doi.org/10.3390/nano13111740

Amani, G. K., Azizi, S., Sintwa, N., Mokalane, K., Mohale, K. C., Mudau, F. N. and Maaza, M., Effect of Optimized Precursor Concentration, Temperature, and Doping on Optical Properties of ZnO Nanoparticles Synthesized via a Green Route Using Bush Tea (Athrixia phylicoides DC.) Leaf Extracts, *ACS Omega.,* 7(36), 31658-31666(2022).

Chauhan, D., Kumar, R., Thakur, N. and Kumar, K., Aloe vera-assisted biogenic synthesis of tunable magnesium oxide nanoparticles for enhanced photocatalytic and antibacterial applications, *J. Dispers. Sci. Technol.,* (2024). https://doi.org/10.1080/01932691.2024.2378203

Cullity, B. D. and Stock, S. R., Elements of X-ray Diffraction, 3rd Edition, Prentice Hall, Upper Saddle River, 2001.

Dhineshbabu, N. R., Rajendran, V., Nithyavathy, N. and Vetumperumal, R., Study of Structural and Optical Properties of Cupric Oxide (CuO) Nanoparticles, *Appl. Nanosci.,* 6, 933(2016). http://dx.doi.org/10.1007/s13204-015-0499-2

Fouda, A., Saied, E., Eid, A. M., Kouadri, F., Alemam, A. M., Hamza, M. F., Alharbi, M., Elkelish, A. and Hassan, S. E. D., Green Synthesis of Zinc Oxide Nanoparticles Using an Aqueous Extract of Punica granatum for Antimicrobial and Catalytic Activity, *J. Funct. Biomater.,* 14(4), 205(2023), https://doi.org/10.3390/jfb14040205

International Centre for Diffraction Data. (1997). JCPDS card No. 48-1548. ICDD.

Marwaha, N., Gupta, B. K., Verma, R. and Srivastava, A. K., Facile synthesis and characterization of pH-dependent pristine MgO nanostructures for visible light emission, *J. Mater. Sci.,* 52, 10480–10484(2017). https://doi.org/10.1007/s10853-017-1231-2

Munisha, M., Kumar, S., Gaur, J., Kaushal, S., Dalal, J., Singh, G., Misra, M. and Ahlawat, D. S., Green synthesis of ZnO nanoparticles using Justicia adhatoda for photocatalytic degradation of malachite green and reduction of 4-nitrophenol, *RSC Adv.,* 15(4), 2958-2980(2025). https://doi.org/10.1039/d4ra08632e

Najamul, L., Sattar, A., Omer, M. O., Hafeez, M. A., Khalid, A. R., Mahmood, S., Shabbir, M. A., Ahmed, W., Aleem, M. T., Alouffi, A. and Almutairi, M. M., Biosynthesis and characterization of zinc oxide nanoparticles using Nigella sativa against coccidiosis in commercial poultry, *Sci. Rep.,* 13, 6568(2023), https://doi.org/10.1038/s41598-023-33416-4

Nguyen, D. T. C., Dang, H. H., Vo, D. V. N., Bach, L. G., Nguyen, T. D. and Tran, T. V., Biogenic synthesis of MgO nanoparticles from different extracts (flower, bark, leaf) of Tecoma stans (L.) and their utilization in selected organic dyes treatment, *J. Hazard. Mater.,* 404, 124146(2020). https://doi.org/10.1016/j.jhazmat.2020.124146

Panchal, P., Paul, D. R., Gautam, S., Meena, P., Nehra, S. P., Maken, S. and Sharma, A., Photocatalytic and antibacterial activities of green synthesized Ag-doped MgO nanocomposites towards environmental sustainability, *Chemosphere*, 297, 134182(2022). https://doi.org/10.1016/j.chemosphere.2022.13418

Patil, S. S., Shedbalkar, U. U., Truskewycz, A., Chopade, B. A. and Ball, A. S., Nanoparticles for environmental clean-up: A review of potential risks and emerging solutions, *Environ. Technol. Innovation.,* 5, 10–21(2016). https://doi.org/10.1016/j.eti.2015.11.001

Prashantkumar, S. C., Banakar, A., Puranik, S. N., Kaveeshwar, V., Ravikumar, C. R. and Gayathri, Characterization of ZnO nanoparticles synthesized using probiotic Lactiplantibacillus plantarum GP258, *Beilstein J. Nanotechnol.,* 16, 78-89(2025). https://doi.org/10.3762/bjnano.16.8

Raliya, R., Tarafdar, J. C. and Biswas, P., Enhancing the mobilization of native phosphorus in the Mung bean rhizosphere using ZnO nanoparticles synthesized by fungi, *J. Agric. Food. Chem.,* 64(16), 3111–3118(2016). https://doi.org/10.1021/acs.jafc.5b05224

Ramesh, M., Anbuvannan, M. and Viruthagiri, G., Green synthesis of ZnO nanoparticles using Solanum nigrum leaf extract and their antibacterial activity, *Spectrochim. Acta, Part A.,* 136, 864–870(2015). https://doi.org/10.1016/j.saa.2014.09.105

Rotti, R. B., Sunitha, D. V., Manjunath, R., Roy, A., Borehalli, S. B. M., Alghamdi, S. and Khidir, E. B., Green synthesis of MgO nanoparticles and its antibacterial properties. Frontiers in Chemistry, 11, 1143614(2023). https://doi.org/10.3389/fchem.2023.1143614

Sankar, R., Maheswari, R., Karthik, S., Shivashangari, K. S. and Ravikumar, V., Anticancer activity of Ficus religiosa engineered copper oxide nanoparticles, *Mater. Sci. Eng. C.,* 44, 234–239(2014). https://doi.org/10.1016/j.msec.2014.08.030

Shifa, S., Jose, B., Raphael, R. and Anila, E. I., Synthesis and characterization of copper oxide thin films by double dip method, *IOP Conf. Seri.,* 1070(1), 012011(2021). https://doi.org/10.1088/1757-899X/1070/1/012011

Vella, D. S. C., Ganapathi, R. R., Kumar, E. and Muthuraj, D., Structural, optical, morphological and thermal properties of CuO nanoparticles prepared by sol-gel technique, *J. Nano- Electron. Phy*., 11(5), 05011(2019). https://doi.org/10.21272/jnep.11(5).05011

Xuan, T. T., Bien, T. T. L., Tran, T. V. and Nguyen, T. T. T., Biosynthesis of ZnO nanoparticles using aqueous extracts of Eclipta prostrata and Piper longum: characterization and assessment of their antioxidant, antibacterial, and photocatalytic properties, *Nanoscale Adv.,* 6(19), 4885-4899(2024) https://doi.org./10.1039/D4NA00326H

Zaman, S., Zainelabdin, A., Amin, G., Nur, O. and Willander, M., Efficient catalytic effect of CuO nanostructures on the degradation of organic dyes, *J. Phy. Chemistry of Solids*, 73, 1320–1324(2012). https://doi.org/10.1016/j.jpcs.2012.07.005